AGU PUBLICATIONS

JGR

Journal of Geophysical Research: Atmospheres

RESEARCH ARTICLE
10.1002/2016JD025042

**Key Points:**
- The three-dimensional global distributions of atmospheric temperatures can be retrieved from ATMS observations using a revised algorithm
- The warm core structures of Sandy obtained by using the revised retrieval algorithm have realistic features and no scan-dependent biases
- Sandy's warm core was confined to upper troposphere while intensifying in tropics and extended to entire troposphere when in midlatitudes

**Correspondence to:**
X. Zou,
xzou1@umd.edu

**Citation:**
Tian, X., and X. Zou (2016), ATMS- and AMSU-A-derived hurricane warm core structures using a modified retrieval algorithm, *J. Geophys. Res. Atmos.*, *121*, 12,630–12,646, doi:10.1002/2016JD025042.

Received 5 MAR 2016
Accepted 17 OCT 2016
Accepted article online 19 OCT 2016
Published online 5 NOV 2016



# ATMS- and AMSU-A-derived hurricane warm core structures using a modified retrieval algorithm

**Xiaoxu Tian[1] and Xiaolei Zou[2]**

[1]Department of Atmospheric and Oceanic Science, University of Maryland, College Park, Maryland, USA, [2]Earth Science System Interdisciplinary Center, University of Maryland, College Park, Maryland, USA

**Abstract** The Advanced Technology Microwave Sounder (ATMS) is a cross-track microwave radiometer. Its temperature sounding channels 5–15 can provide measurements of thermal radiation emitted from different layers of the atmosphere. In this study, a traditional Advanced Microwave Sounding Unit-A (AMSU-A) temperature retrieval algorithm is modified to remove the scan biases in the temperature retrieval and to include only those ATMS sounding channels that are correlated with the atmospheric temperatures on the pressure level of the retrieval. The warm core structures derived for Hurricane Sandy when it moved from tropics to middle latitudes are examined. It is shown that scan biases that are present in the traditional retrieval are adequately removed using the modified algorithm. In addition, temperature retrievals in the upper troposphere (~250 hPa) obtained by using the modified algorithm have more homogeneous warm core structures and those from the traditional retrieval are affected by small-scale features from the low troposphere such as precipitation. Based on ATMS observations, Hurricane Sandy's warm core was confined to the upper troposphere during its intensifying stage and when it was located in the tropics but extended to the entire troposphere when it moved into subtropics and middle latitudes and stopped its further intensification. The modified algorithm was also applied to AMSU-A observation data to retrieve the warm core structures of Hurricane Michael. The retrieved warm core features are more realistic when compared with those from the operational Microwave Integrated Retrieval System (MIRS).

## 1. Introduction

Tropical cyclones (TCs) emerge and intensify over the oceans. Only a handful of in situ measurements are available for observing TCs: sparsely distributed buoys, weather stations over islands, ships, in situ temperature sensors equipped on airplanes, and aircraft dropsondes. In comparison, meteorological satellites are able to provide remote sensing observations within and around TCs with high horizontal, vertical, and/or temporal resolutions. Of particular interest for TC observations and numerical weather prediction are infrared and microwave instruments. A polar-orbiting satellite provides global radiance measurements at microwave and infrared frequencies twice daily. A geostationary satellite can provide time-continuous visible and infrared radiance observations within its observing disk centered at its subsatellite point at the equator. The infrared instruments such as Atmospheric Infrared Sounder, Infrared Atmospheric Sounding Interferometer, and Cross-track Infrared Sounder are extremely valuable for providing radiance measurements with thousands of channels for profiling the atmospheric temperature and water vapor with high vertical resolutions [*Janssen*, 1993; *Le Marshall et al*., 2006; *Hilton et al*., 2012; *Chen et al*., 2013]. However, the infrared channels cannot penetrate the clouds except for optically thin clouds (e.g., cirrus), while tropical cyclones are dominated by thick clouds. In contrast, microwave instruments do not provide as many channels as infrared sounders but can provide unique radiance measurements for profiling the atmospheric temperature and water vapor in almost all weather conditions except for heavy precipitation [*Weng et al*., 2003]. Observations from microwave sounders for window channels are also sensitive to cloud liquid water path and ice water path [*Weng and Grody*, 1994; *Ferraro et al*., 1996]. Since the radiances observed by microwave sounders above the top of atmosphere sample atmosphere layers at different altitudes, it is possible to retrieve atmospheric temperatures in the troposphere and stratosphere from the temperature sounding channels. Hence, microwave sounders are unique for observing TCs populated by clouds, and infrared sounders are important for observing TC's environments.

The Suomi National Polar-orbiting Partnership (S-NPP) satellite was successfully launched on 28 October 2011 into a Sun-synchronous orbit with an ascending equator crossing local time of 1:30 P.M. [*Weng et al*., 2012]. The Advanced Technology Microwave Sounder (ATMS) on board S-NPP is a total power cross-track microwave radiometer. It is an advanced successor of both Advanced Microwave Sounding Unit-A (AMSU-A)

**Table 1.** Channel Features of ATMS and AMSU

| Channel No. | | Frequency (GHz) | | NEDT (K) | | Peak WF |
|---|---|---|---|---|---|---|
| ATMS | AMSU | ATMS | AMSU | ATMS | AMSU | (hPa) |
| 1 | | 23.8 | | 0.5 | | Window |
| 2 | | 31.4 | | 0.6 | | Window |
| 3 | | 50.3 | | 0.7 | | Window |
| 4 | | 51.76 | | 0.5 | | 950 |
| 5 | 4 | 52.8 | | 0.5 | 0.25 | 850 |
| 6 | 5 | 53.596 ± 0.115 | | 0.5 | 0.25 | 700 |
| 7 | 6 | 54.4 | | 0.5 | 0.25 | 400 |
| 8 | 7 | 54.94 | | 0.5 | 0.25 | 250 |
| 9 | 8 | 55.5 | | 0.5 | 0.25 | 200 |
| 10 | 9 | 57.29 | | 0.75 | 0.25 | 100 |
| 11 | 10 | 57.29 ± 0.217 | | 1 | 0.4 | 50 |
| 12 | 11 | 57.29 ± 0.322 ± 0.048 | | 1 | 0.4 | 25 |
| 13 | 12 | 57.29 ± 0.322 ± 0.022 | | 1.25 | 0.6 | 10 |
| 14 | 13 | 57.29 ± 0.322 ± 0.010 | | 2.2 | 0.8 | 5 |
| 15 | 14 | 57.29 ± 0.322 ± 0.0045 | | 3.6 | 1.2 | 2 |
| 16 | 15 | 88.2 | 89 | 0.3 | 0.5 | Window |
| | 16 | | 89 | | 0.84 | Window |
| 17 | 17 | 165.5 | 157 | 0.6 | 0.84 | Window |
| 18 | 20 | 183.31 ± 7.0 | 190.31 | 0.8 | 0.6 | 800 |
| 19 | | 183.31 ± 4.5 | | 0.8 | | 700 |
| 20 | 19 | 183.31 ± 3.0 | | 0.8 | 0.7 | 500 |
| 21 | | 183.31 ± 1.8 | | 0.8 | | 400 |
| 22 | 18 | 183.31 ± 1.0 | | 0.9 | 1.06 | 300 |

and Microwave Humidity Sounder (MHS) to provide spectrum samplings from the Earth's surface to the stratosphere. *Kidder et al*. [2000] gave a comprehensive overview of applying AMSU data in estimating TC intensities, retrieving upper tropospheric temperature anomalies, and determining TC precipitation potentials. *Spencer and Braswell* [2001] estimated TC maximum sustained wind (MSW) using the temperature gradient derived from AMSU-A measurement. *Demuth et al*. [2004, 2006] developed algorithms to apply AMSU observations in evaluating the maximum sustained wind (MSW), minimum sea level pressure, and radii of winds of TCs. *Zou et al*. [2013] found consistently positive impacts of assimilating ATMS observations on hurricane track and intensity forecasts. Compared with its predecessors AMSU-A and MHS, ATMS has more channels, improved spatial resolutions, and a wider swath width. It has much smaller gaps between two consecutive ATMS swaths than AMSU-A swaths in the low latitudes. Given the above mentioned advantages of ATMS over AMSU-A, ATMS can provide a much better depiction of the thermal structures associated with TCs than AMSU-A. The microwave temperature sounding observations from ATMS on board the S-NPP satellite will be used for deriving the warm core structures of TCs in this study [*Weng et al*., 2012; *Zhu and Weng*, 2013].

*Zhu et al*. [2002] proposed an atmospheric temperature retrieval algorithm for AMSU-A observations. Based on the fact that AMSU-A brightness temperatures at temperature sounding channels respond linearly to the temperature within various atmosphere layers, they successfully applied a linear regression atmospheric temperature retrieval algorithm for obtaining warm core structures of hurricanes in the middle and upper troposphere. Recently, *Zhu and Weng* [2013] applied the same temperature retrieval algorithm to ATMS observations to obtain the vertical temperature structures of Hurricane Sandy (2012). They found that unlike a typical TC for which the AMSU-A-retrieved warm core was found in the upper troposphere [*Zhu et al*., 2002], the ATMS-retrieved warm cores of Hurricane Sandy extended throughout the troposphere with quite large horizontal sizes.

The TC's warm core formation, intensification, and structures in the middle and upper troposphere and low stratosphere are closely related to TC evolution. *Galarneau et al*. [2013] investigated the dynamical processes that contribute to the intensifications of Hurricane Sandy during its warm core seclusion. *Dolling and Barnes* [2012] investigated the formation of the TC warm core and its role in the evolution of TCs. Through model simulation, *Zhang and Chen* [2012] showed an important role of the development and intensification of upper level warm core to the rapid intensification (RI) of Hurricane Wilma (2005). The formation of an upper level warm core from the descending air of stratospheric origin in the eye was associated with the detrainment of convective bursts in the eyewall. At the completion of RI, the warm core reached its peak magnitude of more than 18 K at the time when the model-predicted Hurricane Wilma achieved the peak intensity. There were cyclonic radial inflows above the upper outflow layer that could have caused the subsidence adiabatic warming. Given the importance of warm core structures on TC intensity changes, satellite microwave temperature soundings can be utilized in vortex initialization of TCs [*Boukabara et al*., 2011; *Kurihara et al*., 1993, 1995; *Wang*, 1995; *Zou and Xiao*, 2000; *Zou et al*., 2013, 2015] for better forecasting and monitoring of TCs.

In this study, the original algorithm developed by *Zhu et al*. [2002] is modified for better capturing TC warm core structures based on the brightness temperature measurements from ATMS. The first modification is to

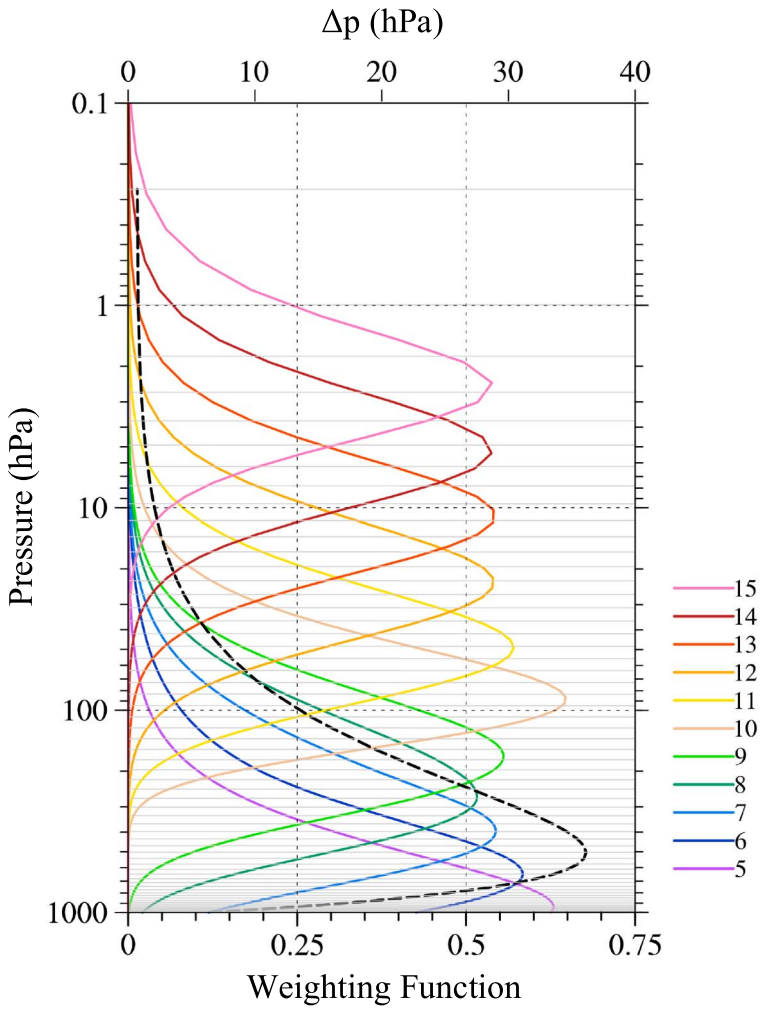


**Figure 1.** Weighting functions of ATMS channels 5–15 (curves in color) and the pressure difference (black dashed curve) between any two neighboring GFS model levels. The 64 GFS model levels are indicated (grey horizontal lines). The weighting functions are calculated using the U.S. standard atmosphere.

establish a regression model at each scan angle of ATMS in order to remove scan biases in temperature retrievals. The second modification is to use only the most highly correlated channels for retrieving atmospheric temperatures at each specific pressure level. The revised algorithm is applied to ATMS observations for Hurricane Sandy during its entire life cycle. Section 2 describes some basic channel characteristics of ATMS instrument. Section 3 provides a mathematical description of the traditional and revised temperature retrieval algorithms. In section 4, numerical results of the temporal evolution of Hurricane Sandy's warm core structures and intensity during its life cycle are compared. The results from the proposed retrieval algorithm are also compared with the Microwave Integrated Retrieval System (MIRS) operational products. Summary and conclusions are provided in section 5.

## 2. Data Description

ATMS is a microwave cross-track scanner with a maximum scan angle of 52.7° with respect to the nadir. It has in total 22 channels with center frequencies ranging from 23 to 183 GHz. ATMS channels 1–16 are similar to those of AMSU-A designed for sounding atmospheric temperatures, and channels 17–22 are similar to those of MHS for water vapor sounding. ATMS consists of two antennas: one observes radiation at channels below 60 GHz and the other observes radiation at all remaining channels. The beam widths are 5.2° for channels 1–2, 2.2° for channels 3–16, and 1.1° for channels 17–22. A single scan line of ATMS consists of 96 fields of view (FOVs) sampled at an interval of 8/3 s. Details of the channel characteristics are provided in Table 1.

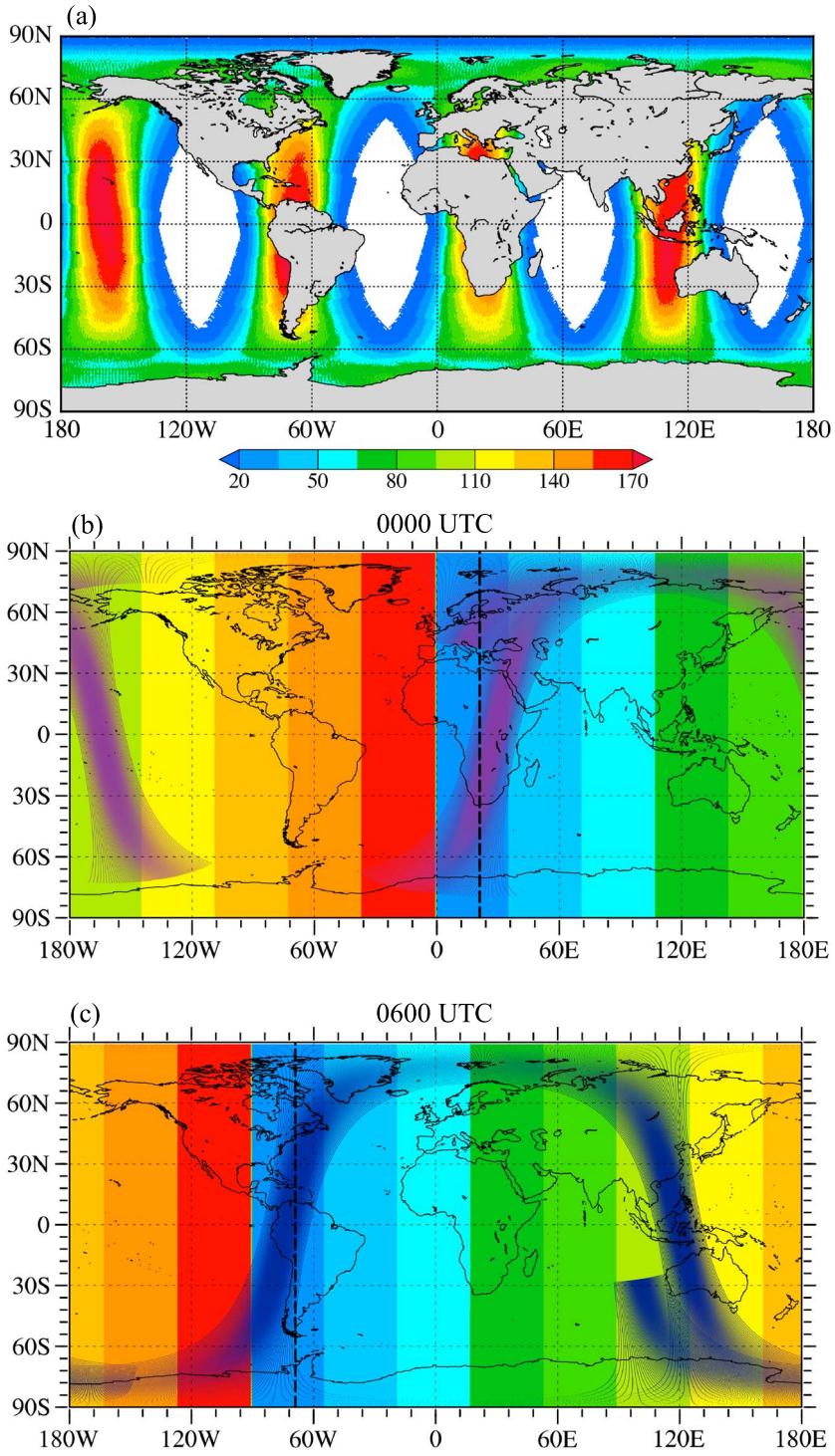


**Figure 2.** (a) Global distribution of the total number of ATMS observations collocated with GFS analysis within 0.5° × 0.5° grid boxes and ±1 h during the time period from 8 to 21 August 2012. ATMS orbits within (b) 0000 ±1 h UTC, (c) 0600 ±1 h UTC, (d) 1200 ±1 h UTC, and (e) 1800 ±1 h UTC, respectively, on 24 October 2012. The meridional dashed line marks the longitude where the local time is 13:30. The color shadings are the global distribution of local time at each UTC time.

Suomi NPP orbits the Earth 14.1875 times each day in a Sun-synchronous, near-circular, and polar orbit that allows ATMS to observe nearly the entire global atmosphere twice daily. Each orbit ascends across the equator at about 1:30 P.M. local time. A single Suomi NPP orbit takes 101.498 min. The repeat cycle is 16 days.

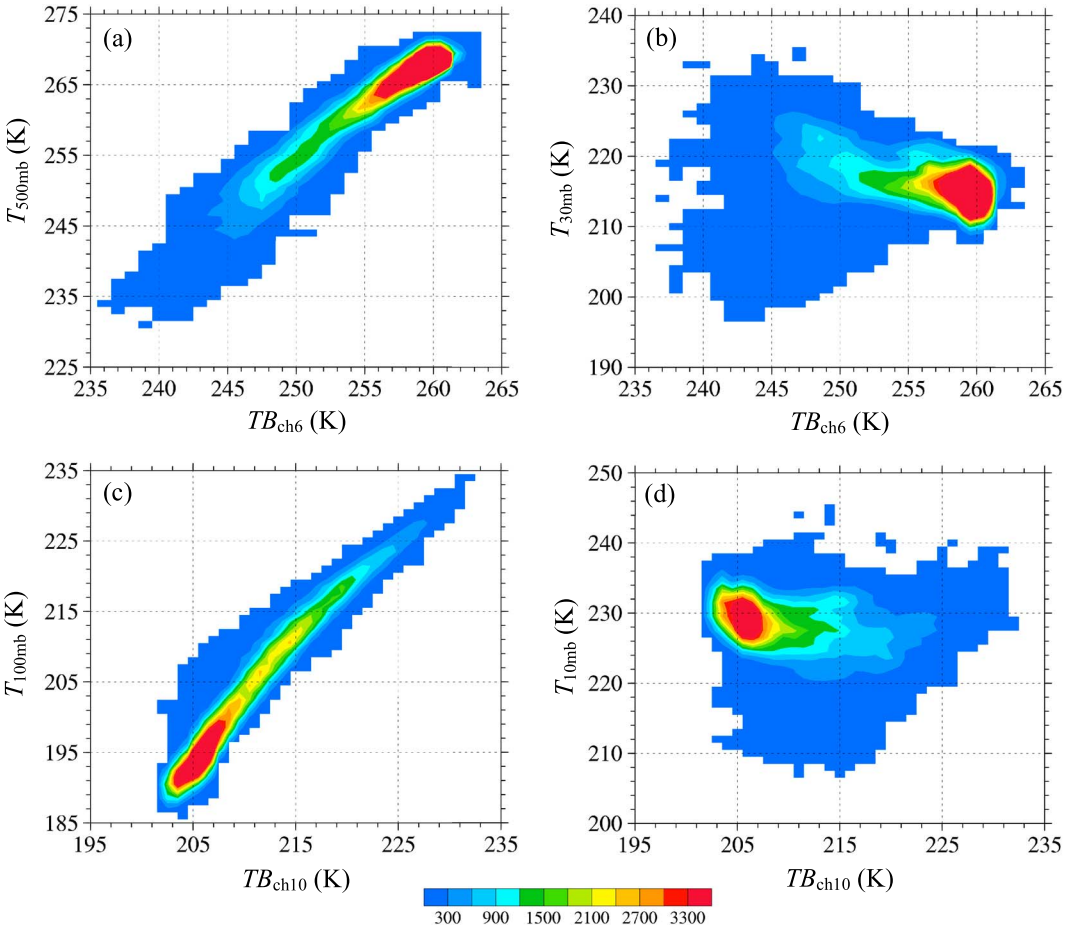


**Figure 3.** Data counts for ATMS brightness temperatures at channel 6 versus GFS temperatures at (a) 500 hPa and (b) 30 hPa and ATMS brightness temperatures at channel 10 versus GFS temperatures at (c) 100 hPa and (d) 10 hPa for all collocated data that are expressed in data counts within 1 K × 1 K grid boxes. The correlations and $R^2$ values for a linear regression between the GFS temperatures and brightness temperatures for Figure 3a are 0.9623 and 92.6%, for Figure 3b are −0.3518 and 12.3%, for Figure 3c are 0.9702 and 94.1%, and for Figure 3d are −0.2721 and 7.41%.

Of particular interest to this study are ATMS channels 5–15 whose weighting functions (WFs) shown in Figure 1 are evenly distributed in the vertical throughout the troposphere and low stratosphere. The WF for a specific channel describes the relative contribution to the measured radiance at this channel's frequency made by each atmospheric layer. Also used in this study are the National Center for Environmental Prediction (NCEP) global forecast system (GFS) 6 h forecasts, which have a horizontal resolution of 0.3125° × 0.3125°, a total of 64 vertical levels, and a model top located near 0.01 hPa, as well as European Centre for Medium-Range Weather Forecasts (ECMWF) Interim analysis data with a horizontal resolution of 0.25° × 0.25° and 60 vertical levels.

## 3. A Brief Description of ATMS Temperature Retrieval Algorithm

The atmospheric temperature at a given pressure level can be expressed as a linear combination of brightness temperatures of ATMS temperature sounding channels [*Zhu et al.*, 2002; *Zhu and Weng*, 2013]:

$$T(p) = C_0(p) + \sum_{i=5}^{15} C_i(p) T_b(v_i) + C_{sz}(p) \frac{1}{\cos(\theta)} \tag{1}$$

where $p$ is pressure level, $\theta$ is the sensor zenith angle (i.e., the angle between the Earth view beam and the local normal direction), $v_i$ is the ATMS channel frequency of the $i$th channel ($i = 5, 6, \ldots, 15$), $T_b$ are the brightness temperatures observed by ATMS, and $C_0$, $C_i$, and $C_{sz}$ are the regression coefficients.

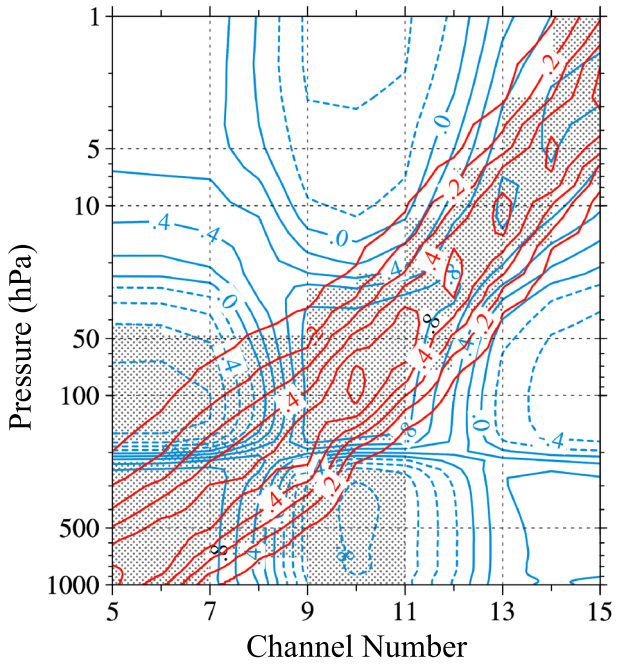


**Figure 4.** Correlations between ATMS brightness temperatures at channels 5–15 and GFS temperatures from surface to 1 hPa (blue curves). Only clear-sky data at nadir (FOVs 48 and 49) are used. Areas with an absolute value of the correlations greater than 0.5 or the weighting functions of ATMS channels 5–15 being greater than 0.1 (shown in red curves) are shaded in grey.

In order to obtain the regression coefficients, the ATMS observations over ocean during the period of 2 weeks prior to Hurricane Sandy, i.e., from 8 to 21 October 2012, are used as a training data set. NCEP GFS atmospheric temperature fields are available at four times, i.e., 0000 UTC, 0600 UTC, 1200 UTC, and 1800 UTC on each day. A global distribution of the total number of ATMS observations collocated with GFS analysis within 0.5° × 0.5° grid boxes and ±1 h during the time period from 8 to 21 October 2012 is provided in Figure 2a.

In equation (1), the regression coefficients $C_0$ and $C_i$ are independent of scan angles, and the last term is included to characterize the scan angle-dependent feature in ATMS observations at temperature sounding channels. However, this last term alone is probably not sufficient for accounting for all the dependencies on zenith angles, causing the retrieved atmospheric temperatures to have scan biases. All observations on the same position of their scan lines, however, are independent from their zenith angles. Therefore, in order to better accommodate the scan dependence, the coefficient training and the temperature retrieval are performed separately at each scan angle instead of once using data from all scan angles. Accordingly, the zenith angle term in equation (1) is removed, while all other terms become functions of scan positions or scan angles. It is also pointed out that observations of all sounding channels 5–15 are included to retrieve atmospheric temperatures at any pressure level. However, the temperatures at a specific pressure level may be correlated to some channels but not all channels. Including those uncorrelated channels could do more damage than help to the retrieval of temperatures at that pressure level. A modified temperature retrieval algorithm is thus proposed that employs the following equation:

$$T(p,\theta) = C_0(p,\theta) + \sum_{i=i_{1,p}}^{i_{2,p}} C_i(p,\theta) T_b(v_i,\theta) \tag{2}$$

where $i_{1,p}$, …, $i_{2,p}$ are a subset of ATMS channels 5–15 that are correlated with the temperature at the pressure level $p$. This algorithm is simpler and computationally more efficient than the one-dimensional variational algorithm called Microwave Integrated Retrieval System (MIRS) [*Boukabara et al.*, 2011]. MIRS is used operationally at NOAA to provide its products to the user community in real time and from the archive.

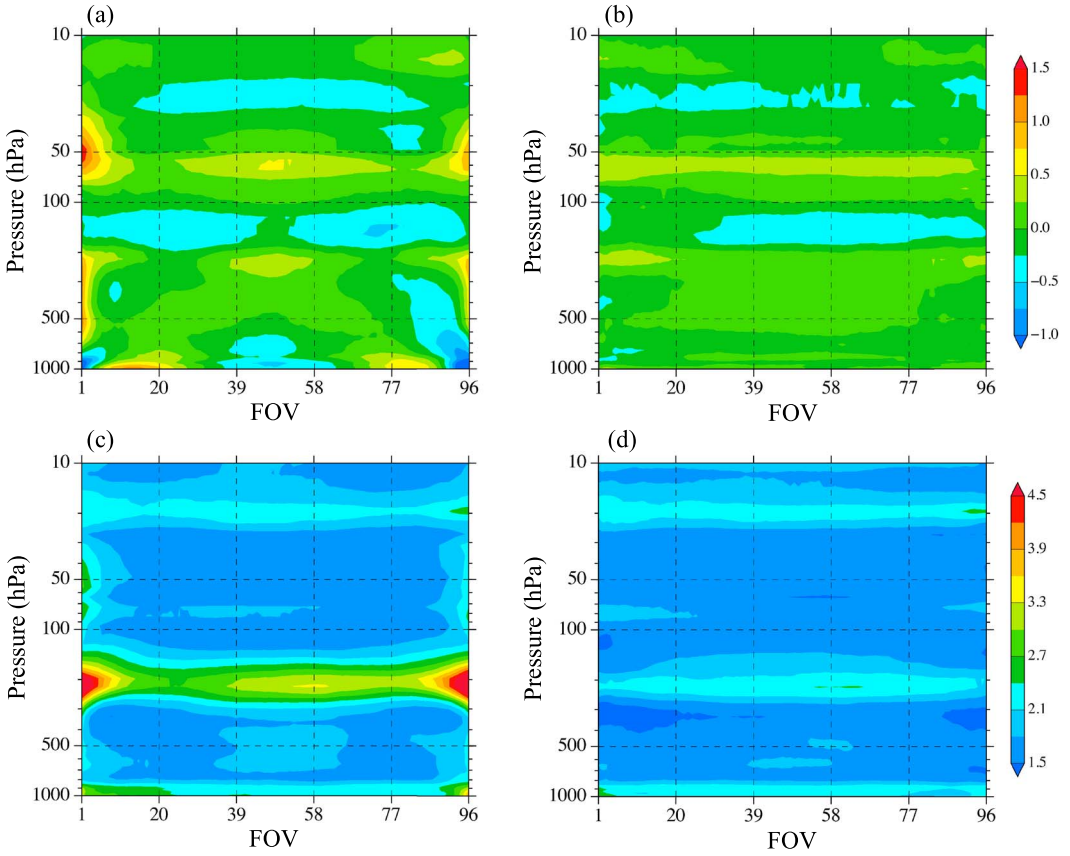


**Figure 5.** (a and b) Biases and (c and d) root-mean-square errors of the temperatures between ATMS retrievals and GFS reanalysis within the period from 22 to 31 October 2012. Figures 5a and 5c are with the traditional algorithm and Figures 5b and 5d with the revised algorithm ($W(p) > 0.1$ or $|\text{corr}| > 0.5$).

## 4. Numerical Results

### 4.1. Refinement of the ATMS Temperature Retrieval

At a given channel, the brightness temperatures do not respond to temperatures at all pressure levels. Figure 3 shows the relationship between ATMS brightness temperatures at channel 6 and GFS temperatures at 500 hPa (Figure 3a) and 30 hPa (Figure 3b) as well as the relationship between ATMS brightness temperatures at channel 10 and GFS temperatures at 100 hPa (Figure 3c) and 10 hPa (Figure 3d) for all collocated data from 10 August to 31 October 2012. ATMS channel 6 is a lower tropospheric sounding channel with its peak WF located at 700 hPa and channel 10 is a stratospheric sounding channel with its peak WF located at 100 hPa. As can be expected, the atmospheric temperatures at 500 hPa (100 hPa) are highly correlated with the ATMS brightness temperatures at channel 6 (channel 10). In contrast, the atmospheric temperatures at 30 hPa (10 hPa) are not correlated with the ATMS brightness temperatures at channel 6 (channel 10) at all. The correlations and $R^2$ values for a linear regression between the GFS temperatures and brightness temperatures for Figure 3a are 0.9623 and 92.6%, for Figure 3b are −0.3518 and 12.3%, for Figure 3c are 0.9702 and 94.1%, and for Figure 3d are −0.2721 and 7.41%.

Correlations between ATMS brightness temperatures at channels 5–15 and GFS temperatures from surface to 1 hPa are provided in Figure 4. Only clear-sky data at nadir (scan positions 48 and 49) are used. Areas with correlations being greater than 0.5 or the weighting functions of ATMS channels 5–15 (shown in red curves) being greater than 0.1 are shaded in grey. At each pressure level, the channels included in equation (2) are either the channels that are correlated with temperatures or the channels whose weighting functions are not negligible at this pressure level, i.e., the channels shaded in grey. At a specific pressure level, those channels that satisfy neither of the criteria are considered "unnecessary" in retrieving the atmospheric

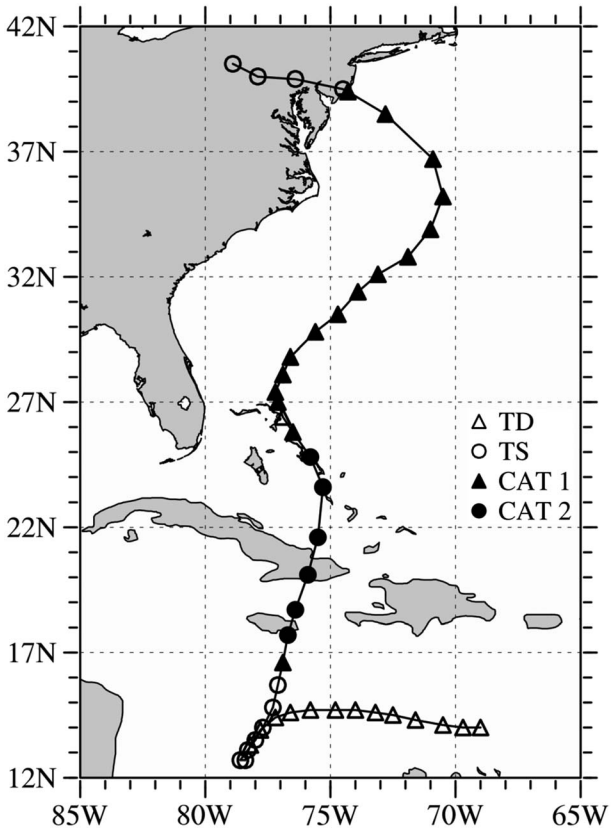


**Figure 6.** The track of Hurricane Sandy from 1200 UTC October 19 to 1800 UTC 30 October 2012, at 6 h interval. Sandy reached a peak intensity of category 3 at 0525 UTC October 2012.

temperatures, as brightness temperatures at these channels convey little information of atmospheric temperatures at the specified pressure level.

The atmospheric temperatures at 64 vertical levels from GFS analysis and the collocated ATMS observation pixels with a ±1 h difference during the period from 8 to 21 October 2012 are included to train the regression coefficients in both the traditional and revised temperature retrieval algorithms. The biases of the atmospheric temperatures between ATMS retrievals and the GFS analysis during the period of Hurricane Sandy (from 22 to 31 October 2012) are shown in Figure 5. A significant scan-dependent bias is found throughout the atmosphere (between 1000 and 10 hPa) for the temperature retrieval using the traditional method (Figure 5a). As was mentioned in section 3, the reason for this is that the last term in equation (1), $C_{sz}(p)\frac{1}{\cos(\theta)}$, for taking account for the scan biases for a cross-track radiometer in the traditional retrieval algorithm does not sufficiently remove the dependencies of ATMS observations on scan angles. In comparison, biases in the temperature retrievals from the revised algorithm are very small ($<\pm 0.5$ K) and have no scan dependence (Figure 5b). Figures 5c and 5d present the root-mean-square (RMS) errors between ATMS-retrieved atmospheric temperatures using the traditional (Figure 5c) and revised (Figure 5d) methods and GFS temperatures ($\sigma = \sqrt{E\left[(T_{\mathrm{GFS}} - T_{\mathrm{ATMS}})^2\right]}$). The revised ATMS temperature retrieval algorithm not only eliminated scan biases but also considerably reduced the variability of the retrieved atmospheric temperatures.

### 4.2. Applications of and Comparisons Between Two Retrieval Algorithms

Hurricane Sandy developed from a tropical wave in the Caribbean Sea on 22 October 2012. It rapidly intensified and became a named tropical storm on the same day. As shown in Figure 6, Hurricane Sandy initially moved westward in the Caribbean Sea then northward over Cuba and Bahamas and northeastward when entering middle latitudes. Hurricane Sandy intensified to a category 1 hurricane

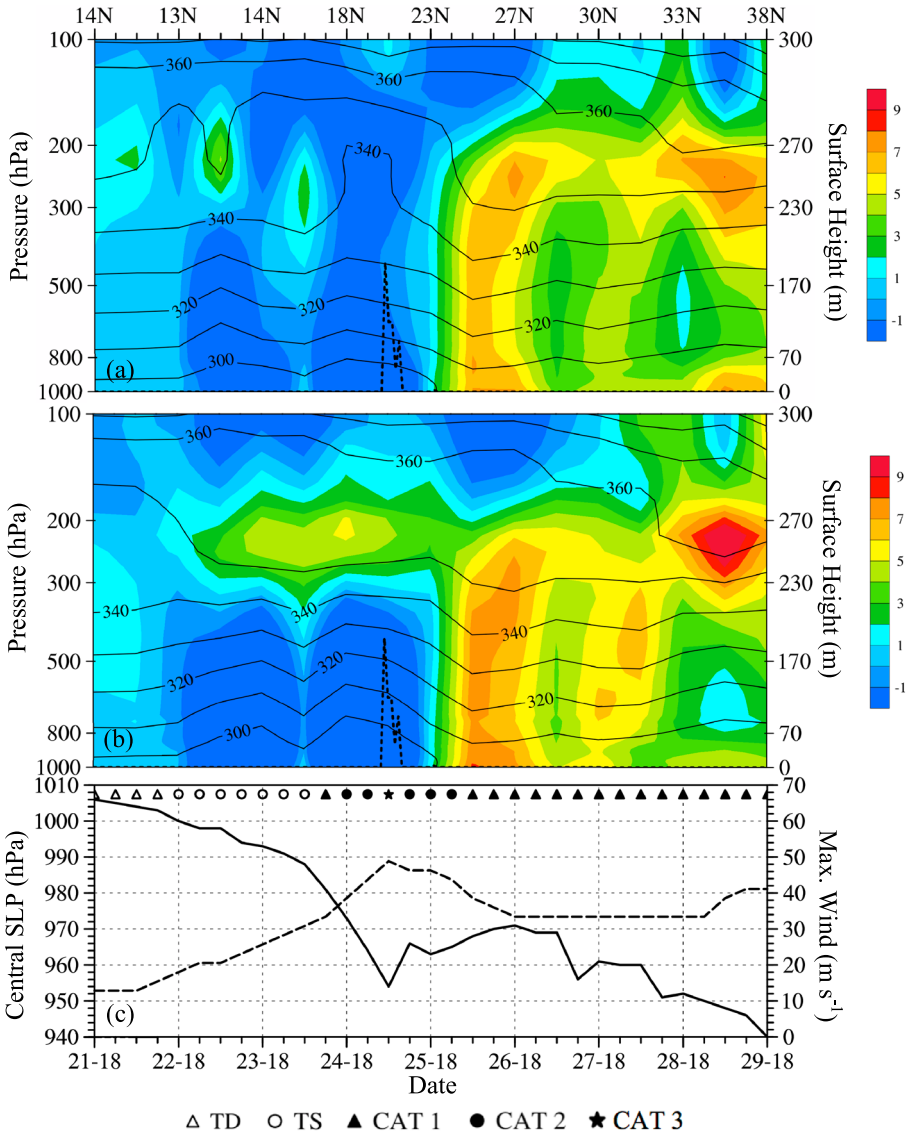


**Figure 7.** Temporal evolution of temperature anomalies (shaded) and potential temperatures (contour) at the center of Hurricane Sandy using the (a) traditional and (b) revised algorithms and (c) the central SLP (solid) and maximum sustained surface wind (dashed) of Hurricane Sandy from the best track data. The terrain height is indicated by dashed curve in Figures 7a and 7b.

on 24 October and further to a category 3 prior to landfall in Cuba. Instead of continuing its northeastward movement, Sandy curved northwestward between 28 and 29 October 2012 and made its landfall on 30 October 2012.

The atmospheric temperature and anomalies throughout the life span of Sandy are retrieved from ATMS observations. Figure 7 shows the temporal and vertical structural evolutions of the temperature anomalies and potential temperatures retrieved with the traditional (Figure 7a) and revised (Figure 7b) algorithms at the hurricane center. The temperature anomalies are defined as the ATMS-retrieved temperatures subtracted by its average temperature within the 15° latitude/longitude box but outside of the 34 knot (17.5 m/s) wind radial distance from the center of the hurricane. The evolution of Sandy's central sea level pressure (SLP) and maximum sustained surface wind obtained from the best track data is shown in Figure 7c. The significant difference in the upper tropospheric warm anomaly between the traditional and revised algorithms is quite stark during 22–25 October 2012 when Sandy evolved from a tropical storm to categories 2 and 3 hurricanes. The revised algorithm gives a consistent warm core structure in

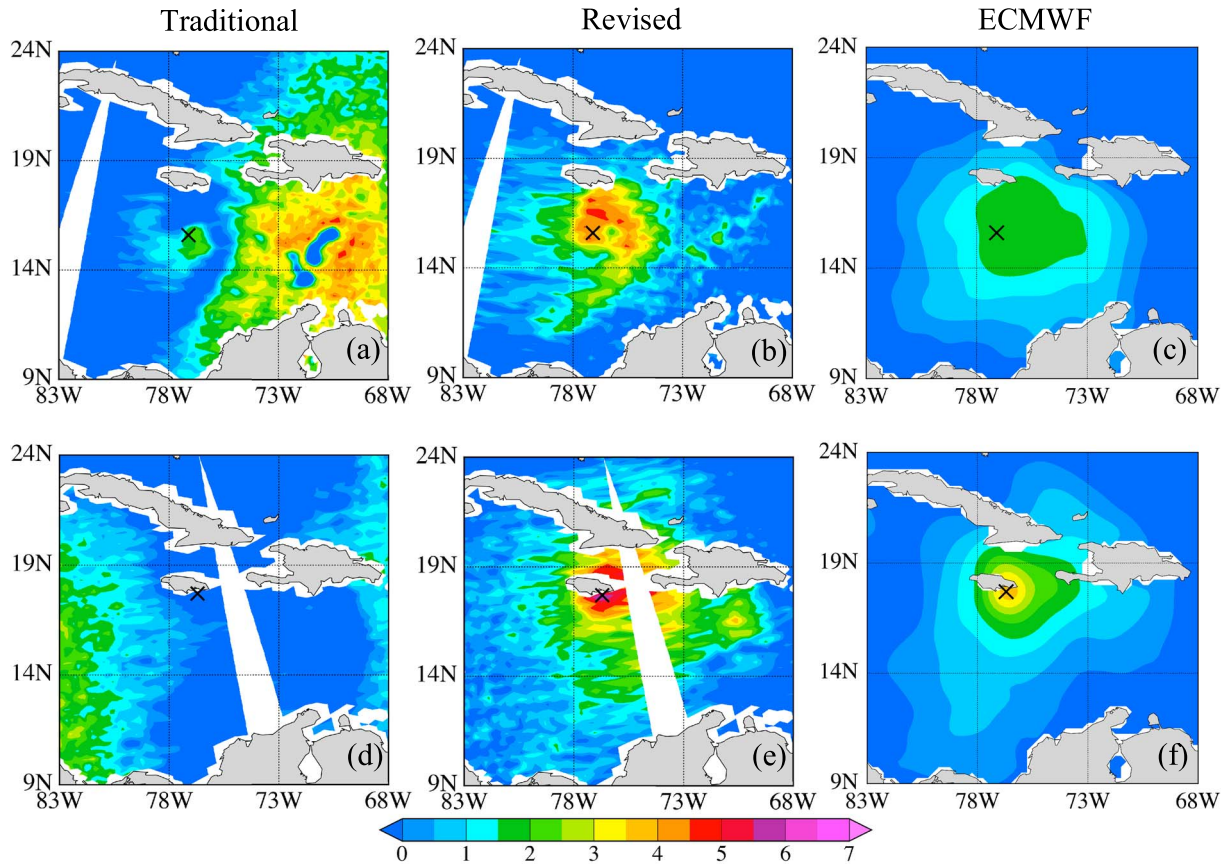


**Figure 8.** Temperature anomalies at 250 hPa at the (a–c) descending (0712 UTC) and (d–f) ascending (1822 UTC) nodes of S-NPP obtained with the traditional (Figures 8a and 8d) and revised (Figures 8b and 8e) ATMS temperature retrieval algorithms, as well as temperature anomalies at 250 hPa of ECMWF Interim at 0600 UTC (Figure 8c) and 1800 UTC (Figure 8f) for Hurricane Sandy on 24 October 2012.

the upper troposphere between 200 and 300 hPa during this period (Figure 7a), which was barely captured by the traditional scheme (Figure 7a). Although being a category 3 hurricane prior to landfall in Cuba, whose terrain height is indicated in Figures 7a and 7b, Sandy experienced a slight weakening moving over Cuba and became a category 2 hurricane. It is noticed that the vertical structures of the temperature anomaly at the center of Sandy are significantly different before and after 1800 UTC 22 October as well as before and after 0600 UTC 26 October 2012. The temperature at the center of the storm initially has a slightly warm anomaly from the ocean surface to 300 hPa from 1800 to 2400 UTC 21 October 2012, during which Sandy remains a tropical depression. A warm anomaly in the upper troposphere and cold anomaly in the middle and lower troposphere developed when Sandy evolved from a tropical depression to tropical storm and intensified and extended to about 200–250 hPa when Sandy intensified more quickly to reach the highest intensity of category 6. At about 0600 UTC 26 October 2012 when Sandy moved into subtropical and middle latitudes, a strong warm anomaly is found throughout the troposphere from the surface to about 200 hPa when Sandy remains a category 1 hurricane.

The horizontal distributions of ATMS-derived temperature anomalies at 250 hPa within Sandy at ATMS descending (0712 UTC) and ascending (1822 UTC) nodes on 24 October 2012 are provided in Figure 8. Figures 8b and 8e are the temperature anomalies calculated with the revised retrieval algorithm, Figures 8c and 8f being the temperature anomalies from ECMWF Interim analysis. At 0600 UTC and 1800 UTC on 24 October, Sandy is classified as tropical storm and category 1 hurricane, respectively. Its warm cores are discernible in the temperature anomalies from ECMWF Interim analysis. However, the temperature anomalies retrieved with both the descending and ascending node observations from traditional algorithm (Figures 8a and 8d) do not provide any warm core structures at 250 hPa, which is due to the scan biases that especially prevails when close to the swath edges as demonstrated in Figure 5. The results

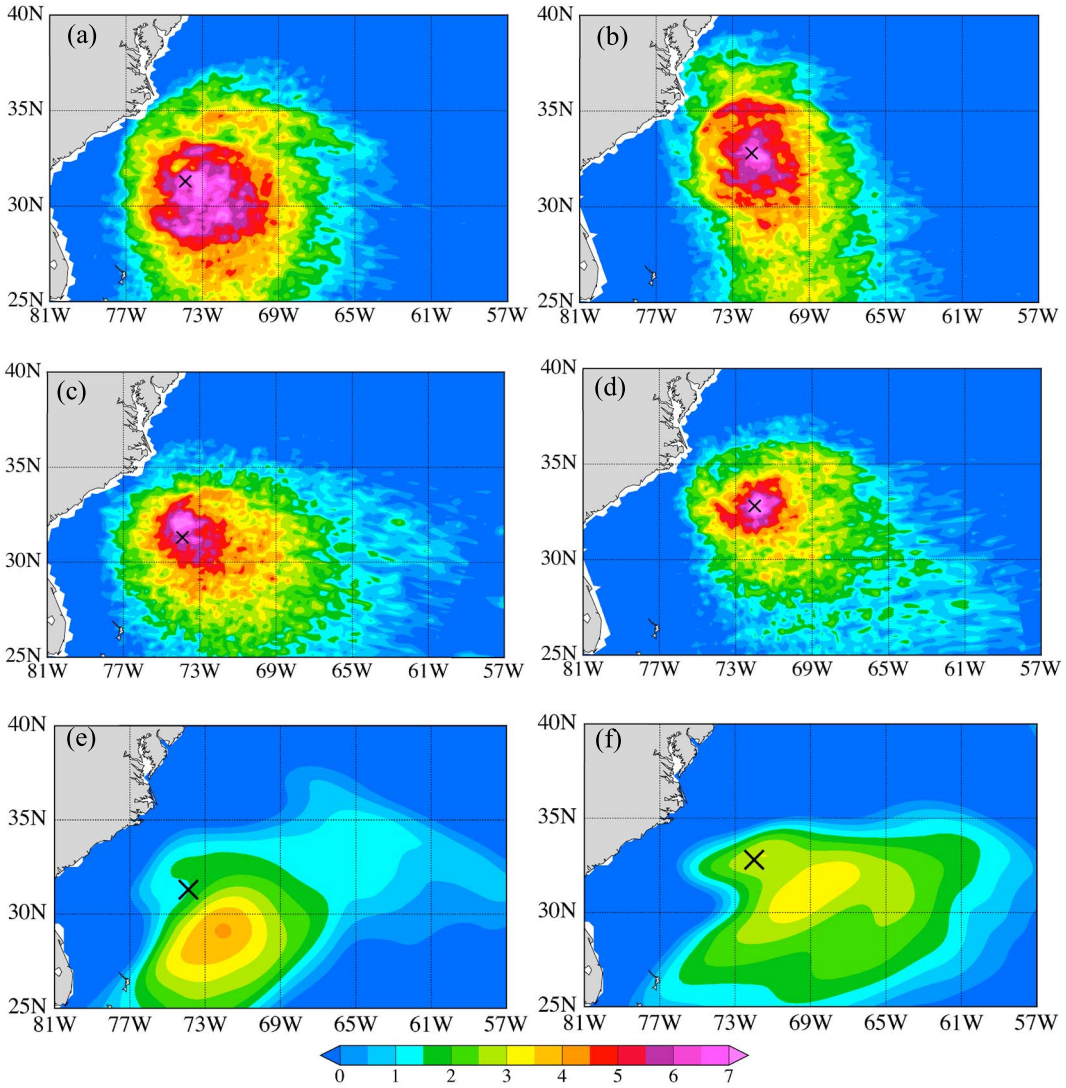


**Figure 9.** Temperature anomalies at 250 hPa at the (a, c, and e) descending (0630 UTC) and (b, d, and f) ascending (1822 UTC) nodes of S-NPP obtained with the traditional (Figures 9a and 9b) and revised (Figures 9c and 9d) ATMS temperature retrieval algorithms, as well as temperature anomalies at 250 hPa of ECMWF Interim analysis at 0600 UTC (Figure 9e) and 1800 UTC (Figure 9f) for Hurricane Sandy on 28 October 2012.

with the same ATMS observations but from revised algorithm can yield warms cores that are much more comparable to those in ECMWF Interim analysis from the perspectives of both shapes and intensities, despite the location of the hurricane center with respect to a swath. Figure 9 demonstrates a similar comparison with Figure 8 only on 28 October. By 28 October, Sandy had entered middle latitudes and developed into a category 1 hurricane. At 250 hPa, the warm core is primarily due to adiabatic heating of the descending air [*Liu et al.*, 1999; *Zhang and Chen*, 2012; *Chen and Zhang*, 2013]. The warm cores at 250 hPa retrieved with traditional method (Figures 9a and 9b) are broader at both the descending (0630 UTC) and ascending (1822 UTC) nodes of S-NPP than those obtained by the revised algorithm. The warm cores in the ECMWF Interim analysis are misplaced to the southeast. It seems that the reanalysis product cannot capture the warm core structure as realistically as satellite observations.

Figure 10 shows the cloud top pressure retrieved from Visible Infrared Imaging Radiometer Suite (VIIRS) observations (Figure 10a) and VIIRS Day Night Band (DNB) radiance (Figure 10b) at 0600 UTC on 28 October. In both the cloud top pressure and VIIRS DNB, Hurricane Sandy is highly asymmetric and the southeast half of the storm area is indicated to be covered with only low-level clouds or even clear sky. Hence, for

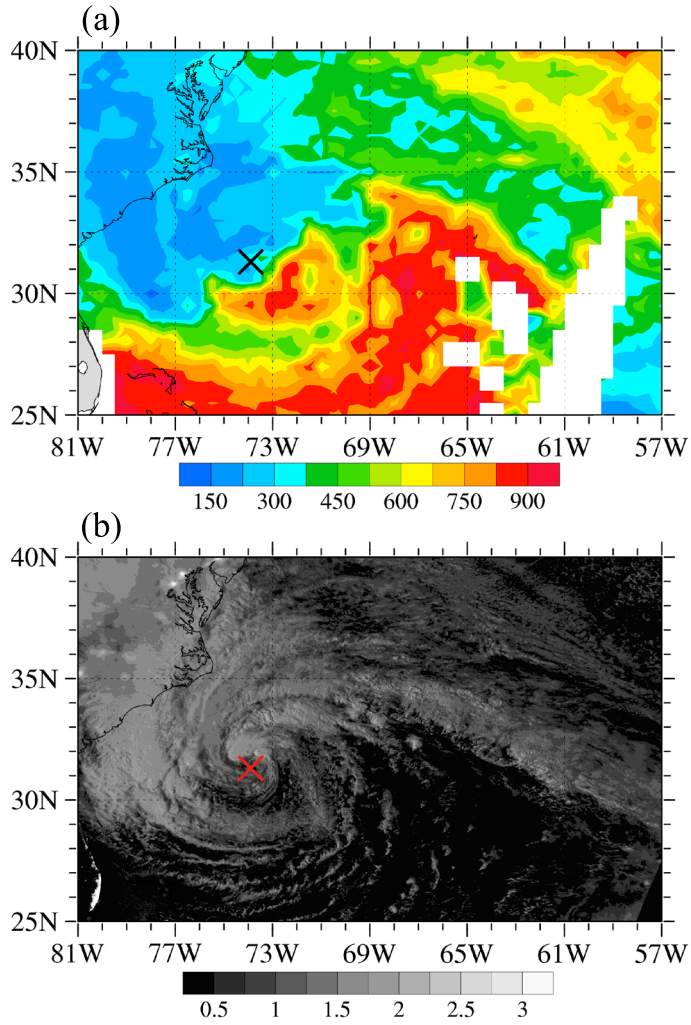


**Figure 10.** (a) Cloud top pressure retrieved from VIIRS observations at 0630 UTC on 28 October 2012. (b) VIIRS DNB radiance (unit: $10^{-8}$ W cm$^{-2}$ sr$^{-1}$) on the descending node (~06:30 UTC) of S-NPP on 28 October 2012.

the southeast half of the storm area, it is certain that convection should have little impact on the temperature field at 250 hPa. The strongest convection was located at the eyewall northwest of the center of Hurricane Sandy. Using the revised new algorithm, the warm core at this time (Figure 9c) has the maximum temperature anomaly of more than 7 K being located at the same location where the convection is the strongest, i.e., the eyewall northwest of the center of Hurricane Sandy.

On 26 October (Figure 11), Sandy left Cuba and passed the Tropic of Cancer. The warm anomaly was located slightly to the east side of the center and stretched throughout the troposphere. When Sandy reintensified to a well-developed hurricane, the warm core became more dominant in the upper troposphere on 28–29 October 2012, which is caused mainly by adiabatic warming of descending air from upper levels induced by radial inflows along the eyewall. The lower troposphere, nonetheless, also has a warm anomaly east of the center of Sandy, corresponding to a clear atmosphere at this region (see Figure 10). It is worth mentioning that the TC's thermal structure in the lower troposphere between 700 hPa and 500 hPa may not be accurately represented by ATMS or model simulation in the presence of clouds.

In order to compare the results obtained by the proposed revised retrieval algorithm for Hurricane Sandy with the operational MIRS retrievals, we show in Figure 12 the temperature anomalies at 250 hPa on 24 October (Figures 12a and 12b) and 28 October (Figures 12c and 12d) 2012 obtained by MIRS from ATMS at both the descending and ascending nodes of S-NPP, as well as the vertical cross sections of temperature anomalies along the constant latitude passing through the center of Hurricane Sandy at 1800 UTC on 26,

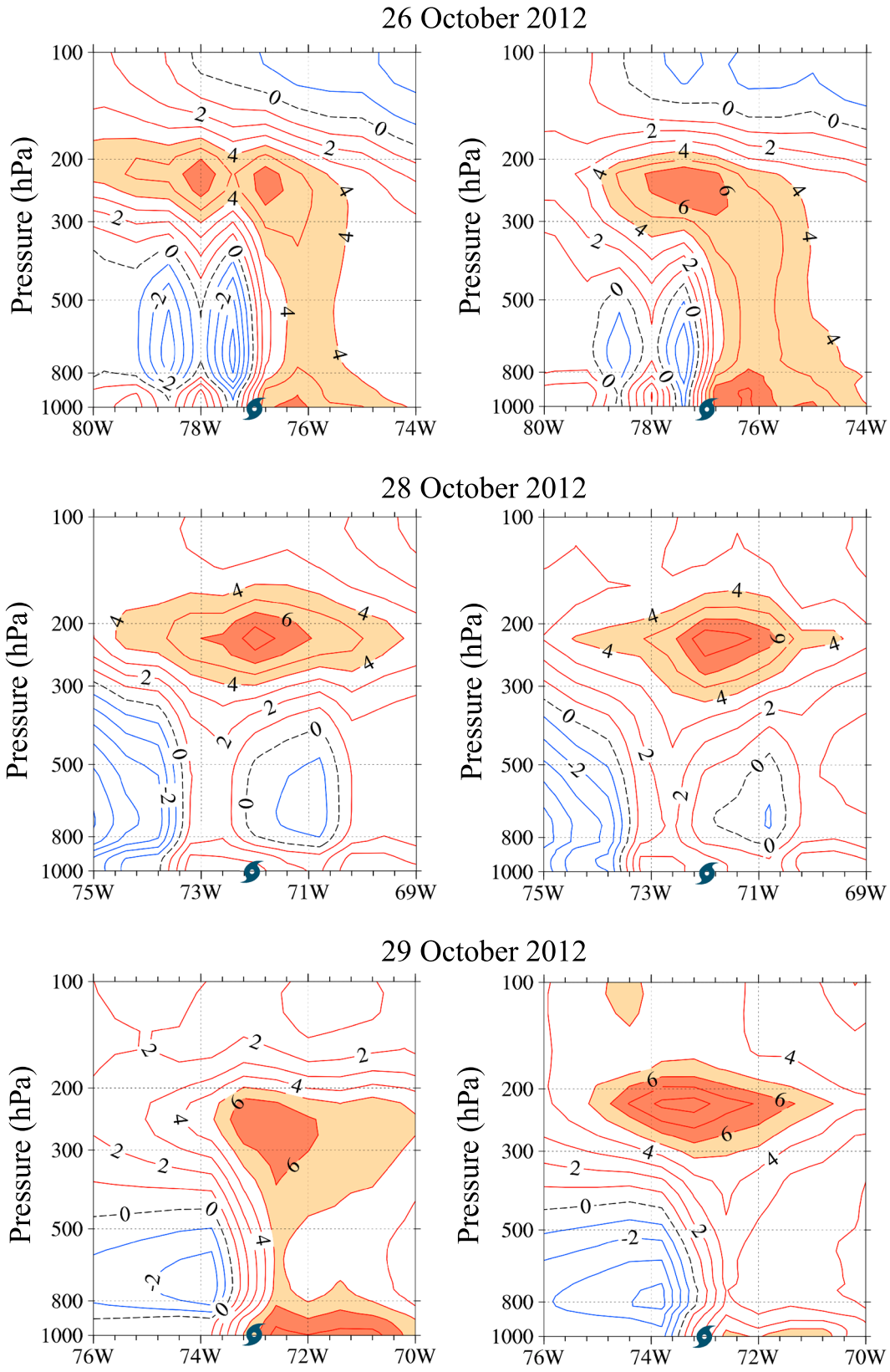


**Figure 11.** Vertical cross sections of temperature anomalies along the constant latitude passing through the center of Hurricane Sandy at 1800 UTC on 26, 28, and 29 October 2012 using the (left column) traditional and (right column) revised algorithms.

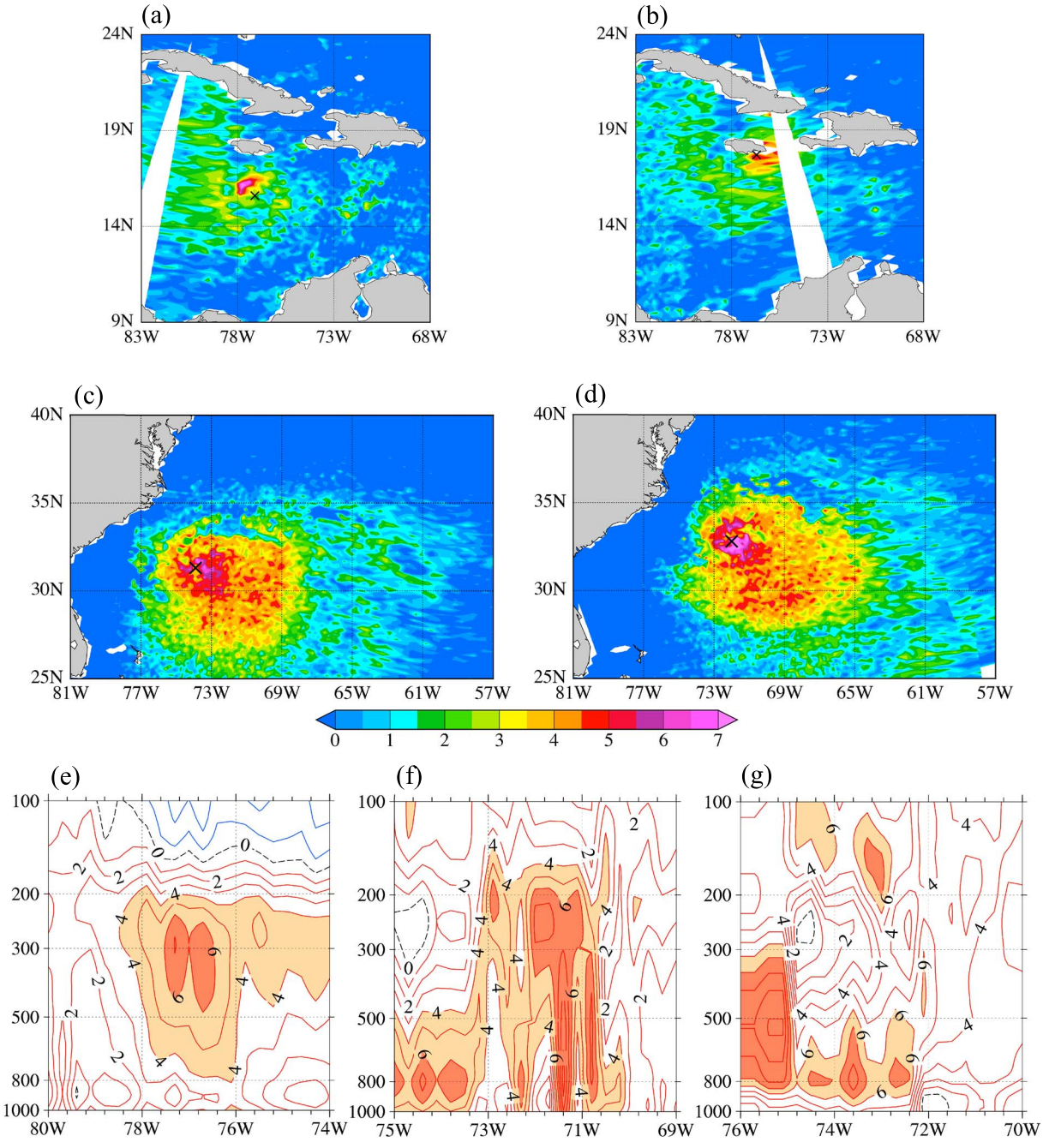


**Figure 12.** Temperature anomalies at 250 hPa on (a and b) 24 October and (c and d) 28 October 2012 obtained by MIRS from ATMS at the descending (Figures 12a and 12c) and ascending (Figures 12b and 12d) nodes of S-NPP. (e–g) Same as Figure 11 except for MIRS results.

28, and 29 October 2012. The warm cores obtained from the MIRS operational retrievals on both 24 (Figures 12a and 12b) and 28 (Figures 12c and 12d) October 2012 are weaker and have smaller spatial scales than the temperature anomalies retrieved by the new algorithm (Figures 8b, 8e, 9c and 9d). The vertical cross sections of the MIRS warm anomalies through the center of Hurricane Sandy along the constant latitude at 1800 UTC on 26, 28, and 29 October 2012 are quite different from those from the traditional and revised retrieval algorithms (Figure 11). The temperature anomalies obtained by the MIRS have features of smaller scales than those from the traditional and revised retrieval algorithms.

Hurricane warm core retrievals are made publicly available by the operational one-dimensional variation Microwave Integrated Retrieval System (MIRS). The MIRS retrievals are based on AMSU-A observations.

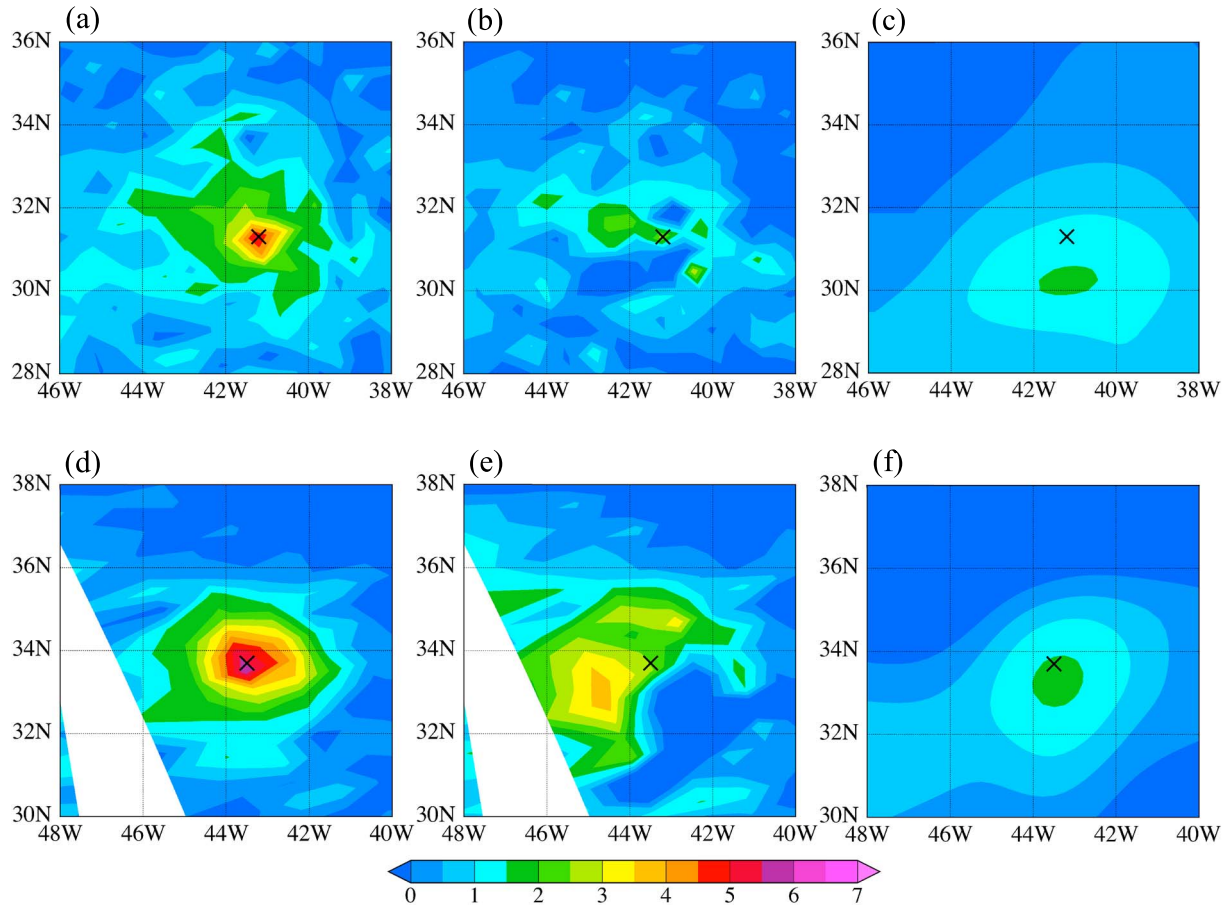


**Figure 13.** Temperature anomalies at 250 hPa from AMSU-A on board NOAA 18 at (a and b) 1800 UTC 7 September (hurricane category 2) and (d and e) 1800 UTC 9 September (hurricane category 1) 2012 using the revised warm core retrieval algorithm (Figures 13a and 13d) and from MIRS (Figures 13b and 13e). Temperature anomalies at 250 hPa of ECMWF Interim analysis at (c) 1800 UTC 7 September 2012 and (f) 1800 UTC 9 September 2012 for Hurricane Michael. The black cross indicates the center of Hurricane Michael which was located at (31.3°N, 41.2°W) for Figures 13a and 13b and (33.7°N, 43.5°W) for Figures 13c and 13d.

In order to compare with the more sophisticated MIRS, the proposed revised retrieval algorithm is applied to AMSU-A on board NOAA 18. Since ATMS channels 5–15 involved in the new modified retrieval algorithm are the same as AMSU-A channels 4–14, the same channel selection is used for the AMSU-A warm core retrieval using the proposed algorithm. Numerical results are then compared between the two algorithms for the warm core structures of Hurricane Michael (2012), which was a named storm at 0600 UTC 4 September 2012. Same as Sandy, a 2-week training period from 15 to 29 August 2012 is used for the regression of the modified scheme when it is applied to Hurricane Michael. Figure 13 provides the temperature anomalies at 250 hPa in the hurricane core obtained by the revised algorithm and those from the MIRS retrievals at 1800 UTC 7 September and 1800 UTC 9 September 2012. Hurricane Michael had a hurricane intensity of category 2 at 1800 UTC 7 September and category 1 at 1800 UTC 9 September, respectively. At both times the revised algorithm is able to retrieve a well-defined warm core structure in the upper troposphere. The warm cores obtained from the MIRS retrievals are much weaker and have a less coherent structure. Similar to the Hurricane Sandy case, it seems that the reanalysis product also cannot capture the warm core structure of Hurricane Michael as realistically as satellite observations.

The vertical cross sections from west to east across the center of Hurricane Michael for the same two times shown in Figure 13 are provided in Figure 14. Hurricane Michael from the revised algorithm (Figures 14a and 14c) had a well-defined warm core in the upper troposphere and a cold core below the warm core. The MIRS retrievals (Figures 14b and 14d) differ greatly from those obtained by the proposed algorithm and did not give a typical warm core feature for a hurricane at categories 1 and 2.

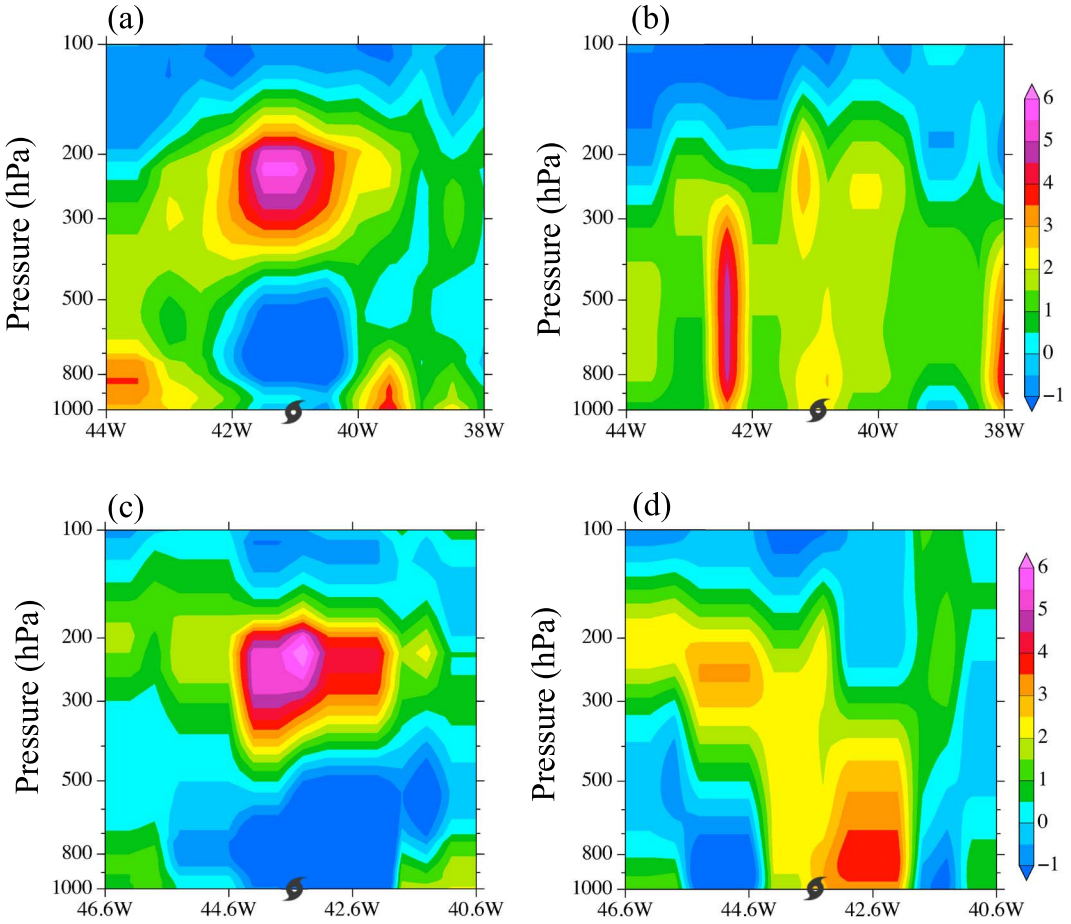


**Figure 14.** Same as Figure 13 except for cross sections from west to east at the latitudes of the center of Hurricane Michael.

## 5. Summary and Conclusions

The improved observing capability of ATMS can be readily applied to monitoring critical weather events such as hurricanes. The temperature retrieval algorithm proposed in previous studies is further improved in order to more accurately retrieve atmospheric temperatures with ATMS observations. As a cross-track microwave scanner, ATMS observations naturally have scan biases, which are found to affect the retrieved temperatures at different pressure levels. To resolve this issue, the regression coefficient training and retrieval process is performed at each individual scan positions. Accordingly, the retrieved atmospheric temperatures from the revised algorithm show no biases related to scan position. The temperature sounding channels of ATMS respond linearly to atmospheric temperature over specific ranges of pressure levels, which is essentially what the weighting function implies. At any pressure level where a given channel's weighting function is close to zero, the atmospheric temperatures and the brightness temperatures turn out to have little correlation. Including all channels in retrievals can even have negative impacts on the accuracies of the retrieved temperatures. In this study, the temperatures in the upper troposphere retrieved when all channels are included are influenced by low-level convection even when convection is absent at upper levels. Therefore, it is not desired to have all temperature sounding channels involved at retrievals of every pressure level. In this study, the involvement of channels at a given pressure level is determined based on the channel's weighting function values and the correlations between the brightness temperature observations at this channel and the atmospheric temperatures at the given pressure level.

With these refinements incorporated into the retrieval algorithm, the retrieved atmospheric temperatures turn out to be unbiased with respect to scan position and with more accuracy when compared with the

temperature fields in GFS analysis. The observations covering the period of Hurricane Sandy when it is located in both the tropics and mid-latitudes are examined with the traditional and revised retrieval algorithms, respectively. It is found that the revised algorithm can capture the asymmetric warm core structures of Hurricane Sandy despite the storm's position within a swath. The warm cores retrieved at upper troposphere are more homogenous compared with the traditional algorithm. The warm core features from the revised method applied to ATMS and AMSU-A observations on board S-NPP and NOAA 18 are compared with the warm cores calculated with temperature profiles retrieved with the same instrument from the operational MIRS retrieval for Hurricane Sandy (2012) and Hurricane Michael (2012), respectively. It was shown that the horizontal and vertical structures of warm cores from the revised new algorithm are more realistic than those from the MIRS operational retrieval. In the future, the retrieved temperatures at stratosphere levels will be examined, as channels 9–15 of ATMS have their peak weighting functions at levels above 200 hPa.

**Acknowledgments**
The authors thank NOAA's Comprehensive Large Array-data Stewardship System (CLASS) for providing observational data (http://www.class.ncdc.noaa.gov/saa/products/welcome), National Center for Environmental Prediction (NCEP) for providing GFS forecasts (http://www.nco.ncep.noaa.gov/pmb/products/gfs/), and ECMWF (http://www.ecmwf.int/en/research/climate-reanalysis/era-interim) for providing ERA-Interim Reanalysis data sets. This work is jointly supported by NOAA Hurricane Forecast Improvement Program (NA15NWS4680002) and Joint Polar Satellite System (NA11OAR4320199). The data used for this paper can be obtained by e-mailing to xzou1@umd.edu.

## References

Boukabara, S.-A., et al. (2011), MiRS: An all-weather 1DVAR satellite data assimilation and retrieval system, *IEEE Trans. Geosci. Remote Sens.*, *49*, 3249–3272.

Chen, H., and D.-L. Zhang (2013), On the rapid intensification of Hurricane Wilma (2005). Part II: Convective bursts and the upper-level warm core, *J. Atmos. Sci.*, *70*, 146–162.

Chen, Y., Y. Han, and F. Weng (2013), Detection of Earth-rotation Doppler Shift from Suomi National Polar-Orbiting Partnership Cross-track Infrared Sounder, *Appl. Opt.*, *52*, 6250–6257.

Demuth, J. L., M. DeMaria, J. A. Knaff, and T. H. Vonder Haar (2004), Evaluation of advanced microwave sounding unit tropical-cyclone intensity and size estimation algorithms, *J. Appl. Meteorol.*, *43*, 282–296.

Demuth, J. L., M. DeMaria, and J. A. Knaff (2006), Improvement of advanced microwave sounding unit tropical cyclone intensity and size estimation algorithms, *J. Appl. Meteorol. Climatol.*, *45*, 1573–1581.

Dolling, K., and G. M. Barnes (2012), Warm-core formation in tropical storm Humberto (2001), *Mon. Weather Rev.*, *140*, 1177–1190.

Ferraro, R. R., F. Z. Weng, N. C. Grody, and A. Basist (1996), An eight-year (1987–1994) time series of rainfall, clouds, water vapor, snow cover, and sea ice derived from SSM/I measurements, *Bull. Am. Meteorol. Soc.*, *77*(5), 891–905.

Galarneau, T. J., Jr., C. A. Davis, and M. A. Shapiro (2013), Intensification of Hurricane Sandy (2012) through extratropical warm core seclusion, *Mon. Weather Rev.*, *141*, 4296–4321.

Hilton, F., et al. (2012), Hyperspectral Earth observation from IASI: Five years of accomplishments, *Bull. Am. Meteorol. Soc.*, *93*(3), 347–370, doi:10.1175/BAMS-D-11-00027.1.

Janssen, M. A. (1993), *Atmospheric Remote Sensing by Microwave Radiometry*, *Wiley Ser. Remote Sens.*, 572 pp., John Wiley, Hoboken, N. J.

Kidder, S. Q., M. D. Goldberg, R. M. Zehr, M. DeMaria, J. F. W. Purdom, C. S. Velden, N. C. Grody, and S. J. Kusselson (2000), Satellite analysis of tropical cyclones using the Advanced Microwave Sounding Unit (AMSU), *Bull. Am. Meteorol. Soc.*, *81*, 1241–1260.

Kurihara, Y., M. A. Bender, and R. Ross (1993), An initialization scheme of hurricane models by vortex specification, *Mon. Weather Rev.*, *121*, 2030–2045.

Kurihara, Y., R. E. Tuleya, and R. Ross (1995), Improvements in the GFDL hurricane prediction system, *Mon. Weather Rev.*, *123*, 2791–2801.

Le Marshall, J., et al. (2006), Improving global analysis and forecasting with AIRS, *Bull. Am. Meteorol. Soc.*, *87*, 891–894.

Liu, Y., D.-L. Zhang, and M. K. Yau (1999), A multiscale numerical study of Hurricane Andrew (1992). Part II: Kinematics and inner-core structures, *Mon. Weather Rev.*, *127*, 2597–2616.

Spencer, R. W., and W. D. Braswell (2001), Atlantic tropical cyclone monitoring with AMSU-A: Estimation of maximum sustained wind speeds, *Mon. Weather Rev.*, *129*, 1518–1532.

Wang, Y. (1995), On an inverse balance equation in sigma coordinates for model initialization, *Mon. Weather Rev.*, *123*, 482–488.

Weng, F., and N. C. Grody (1994), Retrieval of cloud liquid water using the special sensor microwave imager (SSM/I), *J. Geophys. Res.*, *99*(D12), 25,535–25,551, doi:10.1029/94JD02304.

Weng, F., L. Zhao, R. R. Ferraro, G. Poe, X. Li, and N. C. Grody (2003), Advanced microwave sounding unit cloud and precipitation algorithms, *Radio Sci.*, *38*(4), 8068, doi:10.1029/2002RS002679.

Weng, F., X. Zou, X. Wang, S. Yang, and M. Goldberg (2012), Introduction to Suomi NPP ATMS for NWP and tropical cyclone applications, *J. Geophys. Res.*, *117*, D19112, doi:10.1029/2012JD018144.

Zhang, D.-L., and H. Chen (2012), Importance of the upper-level warm core in the rapid intensification of a tropical cyclone, *Geophys. Res. Lett.*, *39*, L02806, doi:10.1029/2012GL052355.

Zhu, T., and F. Weng (2013), Hurricane Sandy warm-core structure observed from Advanced Technology Microwave Sounder, *Geophys. Res. Lett.*, *40*, 3325–3330, doi:10.1002/grl.50626.

Zhu, T., D.-L. Zhang, and F. Weng (2002), Impact of the Advanced Microwave Sounding Unit measurements on hurricane prediction, *Mon. Weather Rev.*, *130*, 2416–2432.

Zou, X., and Q. Xiao (2000), Studies on the initialization and simulation of a mature hurricane using a variational bogus data assimilation scheme, *J. Atmos. Sci.*, *57*, 836–860.

Zou, X., F. Weng, B. Zhang, L. Lin, Z. Qin, and V. Tallapragada (2013), Impacts of assimilation of ATMS data in HWRF on track and intensity forecasts of 2012 four landfall hurricanes, *J. Geophys. Res. Atmos.*, *118*, 11,558–11,576, doi:10.1002/2013JD020405.

Zou, X., Z. Qin, and Y. Zheng (2015), Improved tropical storm forecasts with GOES-13/15 imager radiance assimilation and asymmetric vortex initialization in HWRF, *Mon. Weather Rev.*, *143*(7), 2485–2505.